Influence of bank slope on sinuosity-driven hyporheic exchange flow and residence time distribution during a dynamic flood event

Manuscript submitted to Hydrology and Earth System Sciences

Yiming Li[1,2], Uwe Schneidewind[2], Zhang Wen[1*], Stefan Krause[2], Hui Liu[1]

[1]Hubei Key Laboratory of Yangtze River Catchment Environmental Aquatic Science, School of Environmental Studies, China University of Geosciences, People's Republic of China

[2]School of Geography, Earth and Environmental Sciences, University of Birmingham, UK

***Correspondence:** Zhang Wen (wenz@cug.edu.cn)

Abstract. This study uses a reduced-order two-dimensional (2-D) horizontal model to investigate the influence of riverbank slope on the sinuosity-driven hyporheic exchange process along sloping alluvial riverbanks during a transient flood event. The Deformed Geometry Method (DGM) is applied to quantify the displacement of the sediment-water interface (SWI) along the sloping riverbank during river stage fluctuation. This new modeling approach serves as the initial step focusing on the impact of bank slope on the hyporheic exchange flux (HEF) and the residence time distribution (RTD) of pore water in the fluvial aquifer for a sinuosity-driven river corridor. Several controlling factors, including sinuosity, alluvial valley slope, river flow advective forcing and duration of flow are incorporated into the model to investigate the effects of bank slope on aquifers of variable hydraulic transmissivity. Compared to simulations of a vertical riverbank, sloping riverbanks were found to increase the HEF. For sloping riverbanks, the hyporheic zone (HZ) encompasses a larger area and penetrated deeper into the alluvial aquifer, especially in aquifers with smaller transmissivity (i.e., due to increased hydraulic conductivity or reduced specific yield). Furthermore, consideration of sloping banks as compared to a vertical river bank can lead to both underestimation or overestimation of the pore water travel time. The impact of bank slope on residence time was more pronounced during a flood event for high transmissivity aquifer conditions, while it had a long-lasting influence after the flood event in lower transmissivity aquifers. Consequently, this decreases the travel time of water discharging into the river relative to base flow conditions. These findings highlight the need for (re)consideration of the importance of more complex riverbank morphology as control of hyporheic exchange in floodplains. The results have potential implications for river management and restoration and the management of river and groundwater pollution.

Key words: hyporheic exchange, sloping riverbank, deformed geometry, numerical simulation, residence time distribution

Nomenclature

ΔL	Nodal spacing [m]
∇	Laplace operator
α_L	Longitudinal dispersivity [L]
α_T	Transverse dispersivity [L]
$\mathbf{D}$	Dispersion-diffusion tensor [L^2T^{-1}]
D_L	Water diffusivity [L^2T^{-1}]
J_x	Base groundwater gradient [-]
K	Hydraulic conductivity [LT^{-1}]
n	Scaling number [-]
n_0	Intensity of flood event [-]
n_d	Skewness of flood event [-]
S_y	Specific yield [-]
t_d	Duration of flood event [T]
t_p	Time to peak river stage [T]
α	Amplitude of the river boundary [L]
Γ_d	Dimensionless aquifer transmissivity [-]
δ	Bank slope angle [°]
δ_{ij}	Kronecker delta function [-]
ϵ	Tortuosity [-]
η	Degree of flood event asymmetry[T^{-1}]
θ	Effective porosity [-]
λ	River boundary wave length [L]
σ	River boundary sinuosity [-]
τ	Residence time [T]
ω	Flood event frequency[T^{-1}]
$h(\mathbf{x}, t)$	Transient groundwater head [L]
Δh^*	Dimensionless parameter of ambient groundwater flow [-]

$A^{**}(t)$	Dimensionless variation of HZ area relative to base flow conditions [-]
$C(\mathbf{x}, t)$	Solute concentration in the aquifer [ML^{-3}]
$C_0(\mathbf{x})$	Solute concentration as initial condition [ML^{-3}]
$C_S(\mathbf{x}, t)$	Solute concentration in the river [ML^{-3}]
$d^{**}(t)$	Dimensionless variation of HZ penetration distance relative to base flow conditions [-]
$H(\mathbf{x}, t)$	Thickness of the saturated aquifer [L]
$H_0(\mathbf{x})$	Initial river stage [L]
H_p	Peak river stage during the flood event [L]
$H_r(t)$	River stage at the downstream end [L]
$h_r(x, t)$	Transient river stage [L]
$M(t)$	Displacement of the sediment-water interface [L]
P_e	Péclet number [-]
$\mathbf{q}$	Specific discharge or Darcy flux [LT^{-1}]
$\mathbf{Q}$	Aquifer-integrated discharge [L^2T^{-1}]
$Q^*_{in,\,HZ}(t)$	Dimensionless net flux along the river boundary [-]
$Q^*_{in,\,HZ}(t)$	Dimensionless exchange flux from the aquifer to the river [-]
$Q^*_{out,\,HZ}(t)$	Dimensionless exchange flux from the river to the aquifer [-]
$Y(x, t)$	Location of the sediment-water interface boundary [L]
$z_b(\mathbf{x})$	Elevation of the underlying impermeable layer [L]
Γ_d	Dimensionless parameter of aquifer transmissivity [-]
$\mu(\mathbf{x}, 0)$	Mean (first order of) residence time distribution [T]
$\mu^*_{out}(x, t)$	Flux-weighted ratio of mean RT to mean RT under baseflow conditions [-]
$\mu_n(\mathbf{x}, t)$	n-th moment of residence time distribution [T^n]
$\mu_r^*(\mathbf{x}, t)$	Residence time distribution ratio between slope and vertical river bank model [-]
$\mu_{\tau 0\text{-max}}$	Maximum RT in the domain [T]

$\mu_{\tau\text{-}S}(\mathbf{x}, t)$	Residence time distribution of slope river bank model [T]
$\mu_{\tau\text{-}V}(\mathbf{x}, 0)$	Residence time distribution of vertical river bank model [T]
$\rho(\mathbf{x}, t, \tau)$	Residence time distribution [T]
Abbreviations	
HZ	Hyporheic zone
HEF	Hyporheic exchange flux
DGM	Deformed Geometry Method
SWI	Sediment-water interface
RTD	Residence time distribution
RT	Residence time
ALE	Arbitrary Lagrangian–Eulerian
2-D	Two-dimensional
BTS	Biogeochemical timescale

1. Introduction

The hyporheic zone (HZ) can be described as the region that connects the river channel and adjacent aquifer, and includes riverbed and riverbanks. Mixing and transporting of different water types (groundwater, surface water) and ages in the HZ driven by hydrodynamic and hydrostatic factors cause spatially and temporally varying exchange of water and biogeochemical species between river channel, riverbed and aquifer (Cardenas, 2009b; Hester and Gooseff, 2010; Krause et al., 2011, 2017, 2022; McClain et al., 2013; Boano et al., 2014). The hyporheic exchange flux (HEF) represents the interaction flux between surface water and groundwater in vertical (e.g., bedform-driven) and horizontal (e.g., meander-driven) directions, which can add to general regional groundwater ex-filtration and infiltration. The distribution of hyporheic flow paths strongly determines the spatial and temporal distribution of hydrogeochemical characteristics of water within the riverbed and the wider river corridor as well as the formation of so-called hot zones and hot moments (Krause et al., 2013, 2017; Cardenas, 2015; Pinay et al., 2015).

Hyporheic exchange flux (HEF) is controlled by parameters such as stream discharge dynamics, recharge, riverbed and aquifer hydraulic properties, local hydraulic head fluctuations, as well as river geometry and morphology including sinuosity and riverbank slope (Larkin and Sharp, 1992; Gomez-Velez et al., 2012; 2017; Schmadel et al., 2016). For example, Cardenas et al. (2004) demonstrated how riverbed characteristics and especially the heterogeneity of hydraulic conductivity could increase HEF by 17% to 32%. As such, to be able to better estimate the relative importance of HEF on catchment water fluxes and biogeochemical processes require a good understanding of its different drivers and controls. This is imperative as the spatiotemporal evolution of HEF, the resulting change in HZ (area) and thus also the residence or travel time (RT) of the exchanged water in the HZ have significant impact on flow dynamics and transient storage along the river continuum and in turn control

the capacity for contaminant attenuation (Weatherill et al., 2018) and biogeochemical functions of river corridors (Bertrand et al., 2012; Boulton et al., 2010; Brunke and Gonser, 1997).

Both lateral exchange between river and its floodplain, as well as bedform-induced vertical exchange at the streambed interface have been found to be crucial with regards to HEF and the biogeochemical transformation potential along the river corridor (Boano et al., 2010, 2014; Gomez-Velez and Harvey, 2014; Gomez-Velez et al., 2015, 2017; Kiel and Cardenas, 2014; Stonedahl et al., 2013). Through using numerical simulations, considerable progress has been made with regards to our understanding of how river planform geometry (Boano et al., 2006, 2010; Cardenas 2006; 2008; 2009a, 2009b; Stonedahl 2013), dynamic flood events (Gomez-Velez et al., 2012; 2017) and evapotranspiration (Kruegler et al., 2020) control HEF. Focusing on lateral exchange flow processes, Cardenas (2008; 2009a, 2009b) utilized numerical models to investigate HEF and residence time distribution (RTD) for various river channel morphologies and regional groundwater flow conditions. Their simulations indicate that channel morphology, represented by sinuosity, is a dominant factor controlling HEF, the total HZ area, and RTD. In addition, Boano et al. (2010) used a similar modeling framework to study the relationship between RTD and biogeochemical transformation by introducing surface water as a major source of dissolved organic matter that triggers a sequence of redox reactions within the HZ. Reactive transport simulations showed a good relationship between RTD and denitrification reaction potential. Based on these studies, Gomez-Velez et al. (2012) conducted numerical simulations to investigate the impact of aquifer parameters (water table gradient, hydraulic conductivity, dispersivity) and channel sinuosity on HEF and RTD. By comparing RTD with the timescale of nitrification/denitrification reactions, a meander can be classified as a source or sink of nitrate. More recent modeling studies focused predominantly on the effects of dynamic river/groundwater stage fluctuations on lateral (e.g., Schmadel et al., 2016; Gomez-Velez et al., 2017) and vertical (e.g., Singh et al., 2019, 2020; Wu et al., 2018, 2020,

2021) hyporheic exchange and RTD. For example, Gomez-Velez et al. (2017) explored the HZ response to a dynamic river stage due to variable hydraulic conductivity, groundwater flow gradient and river sinuosity conditions. Their results indicate that the dynamic forcing greatly influences net HEF, the area of HZ and RTD across different scenarios, whereby higher aquifer transmissivity will likely result in a stronger but shorter response of HEF and RTD to a flood event.

Although there is a considerable body of numerical research on the lateral hyporheic response to the various geometrical (e.g., geometry of river channel, river slope, etc) and dynamic drivers (e.g., fluctuation of river/groundwater, gaining and losing conditions of groundwater, etc), many HZ studies do not specifically consider floodplain-driven processes or they apply vertical riverbanks with straight river planimetry in an attempt to reduce model complexity in line with the analytical or numerical solutions used (Cooper and Rorabaugh, 1963; Hunt, 1990; Schmadel et al., 2016; Gomez-Velez et al., 2017;). However, riverbanks are usually sloping (inclined) rather than vertical (Liang et al., 2018) as they undergo erosion (Osma and Thorne, 1988). Previous research has proven that bank erosion and bank collapse are globally spreading processes controlled by various factors, such as initial bank slope angle (Zingg, 1940; Lindow et al., 2009), surface flow forces (Hagerty et al., 1995; Fox and Wilson, 2010), vegetation cover (Mayor et al., 2008; Gao et al., 2009; Puttock et al., 2013) and sediment properties (Millar and Quich, 1993). Neglecting bank slope in analytical and numerical model solutions may therefore have a significant influence on the prediction accuracy of HEF (Doble et al. 2012a, 2012b) and RTD (Derx et al., 2014; Siergieiev et al., 2015) in an unconfined floodplain aquifer. Thus, a detailed analysis of the floodplain drivers of HEF should require a more detailed consideration of the floodplain geometry including riverbank slope in bank storage conceptual models (Sharp, 1977).

A few previous studies have used numerical modeling where the model is bounded by a sloping riverbank to assess the influence of bank slope on HEF for a

vertical section of an alluvial aquifer. In such cases, the aquifer was considered variably saturated, homogenous, and isotropic, while flow in the unsaturated zone was calculated using the Richards equation (Li et al., 2008; McCallum et al., 2010; Doble 2012a; b). These studies have confirmed that neglecting bank slope can lead to an underestimation of the bank storage volume as well as the temporal HEF in vertical cross-sectional profiles, especially under relatively small bank angles.

In turn, river sinuosity and ambient groundwater gradient (along the river channel) have not been studied as potential drivers of sinuosity-driven lateral HEF and RTD and their biogeochemical implications when a sloping river bank exists and it needs to be determined whether considering both drivers can lead to significantly different findings as compared to previous cross-sectional profile models (Doble et al., 2012; Siergieiev et al., 2015; Derx et al., 2014). In this study, we therefore quantify the effect of bank slope on the spatial extent (area) of the HZ in sinuosity-driven river meanders and how it impacts the evolution of HEF and RTD under varying aquifer transmissivity conditions to better understand lateral HEF through the alluvial plain. We build on the numerical modeling approach introduced by Gomez-Velez et al. (2017) and consider lateral bank slope by coupling the deformed geometry method (DGM) to the flow (Liang et al. 2020), the solute transport and the residence time distribution equation. Our results reveal how and when bank slope plays an important role in sinuosity-driven meandering rivers with respect to HEF and RTD, which in turn will lead to an improved understanding of the river channel-aquifer-floodplain system and provide guidance on the placement of monitoring locations in river management studies.

2. Methodology

2.1 Model setup using deformed geometry method

The modeling approach and dimensionless parameterization metrics used by Gomez-Velez et al. (2017) can represent most riverbank-aquifer situations and dynamic flood conditions. In our study, we use their conceptual model to set up a baseline case with the same model frame, equations and parameterization metrics. Additional information regarding the implementation of this baseline case can be found in the SI. However, where their previous research assumed a vertical river bank for sinuosity-driven HEF models, we consider a sloping riverbank and use the DGM approach to capture the dynamic evolution of the SWI along the river course. A constant sloping angle (δ [°]) along the alluvial riverbank of a sinusoidal river was implemented in our model (see blue lines of conceptual model in Figure S1 and the corresponding mathematical model in Figure S2a) while the surface water interface (SWI) was assumed to be always vertical (vertical solid red and green lines in Figure S2c). As such, the contraction or expansion of the simulated domain, i.e., displacement of the SWI can be characterized by the sloping angle (there is no movement of the SWI for the vertical riverbank case) and river stage. As the river stage changes, so does the location of the SWI.

When the river stage changes in our model, the sinusoidal boundary will migrate towards or away from the floodplain meaning that the submerged part of the riverbank is considered contracted and our model only considers the alluvial aquifer that is not submerged. The evolution of the SWI during a flood event can be calculated by considering river stage and bank slope via:

$$Y(x, t) = Y_0(x) + M(t) \quad (1)$$

where $Y(x, t)$ [L] is the location of the SWI boundary while $Y_0(x)$ [L] is the initial

location of the SWI. In contrast to Gomez-Velez et al. (2017), the displacement of the SWI caused by the deformation of the model domain ($M(t) = [h(t) - h(0)]/\tan(\delta)$, where $h(t)$ [L] is transient hydraulic head) is added in Eq. (1), which represents the displacement of the river boundary in y-direction due to river stage fluctuation and bank slope angle (see the horizontal distance between the vertical red and green solid line in Figure S2c).

To simulate the model domain deformation and mesh displacement, we use the DGM interface in COMSOL. In this interface, the deforming feature of a specified domain can be defined as a boundary condition with a given moving velocity or displacement. DGM is based on the arbitrary Lagrangian–Eulerian (ALE) method, which is a hybrid method that allows both the model domain and mesh to move or deform simultaneously in a predefined manner. More details on ALE can be found in Donea et al. (2014). While it has previously been used for simulating general free-surface problems (e.g., Duarte et al., 2004; Maury, 1996; Pohjoranta and Tenno, 2011), to our knowledge, DGM has not yet been implemented to solve moving boundary problems in hyporheic exchange studies. Here we used Eq. (1) as an input to the DGM interface to simulate the displacement of the SWI (water flow) during a dynamic flood event. Infiltration and seepage face before and after the peak time of the flood event, respectively, were neglected (Boano et al., 2006; Cardenas. 2009a, b; Kruegler et al., 2020). Fig. 1 illustrates the river stage hydrograph of this study (Fig. 1a, calculated by Eq. (S2)) and the diagram of the displacement of the SWI (Fig. 1b) during the flood event after coupling DGM into the model. The colored river boundaries in Fig. 1b are corresponding to the times of colored dots in Fig. 1a. Additionally, solute transport and RTD were simulated based on the extent of the flow field according to Gomez-Velez et al. (2017), as shown in the SI (S2 and S3, respectively).

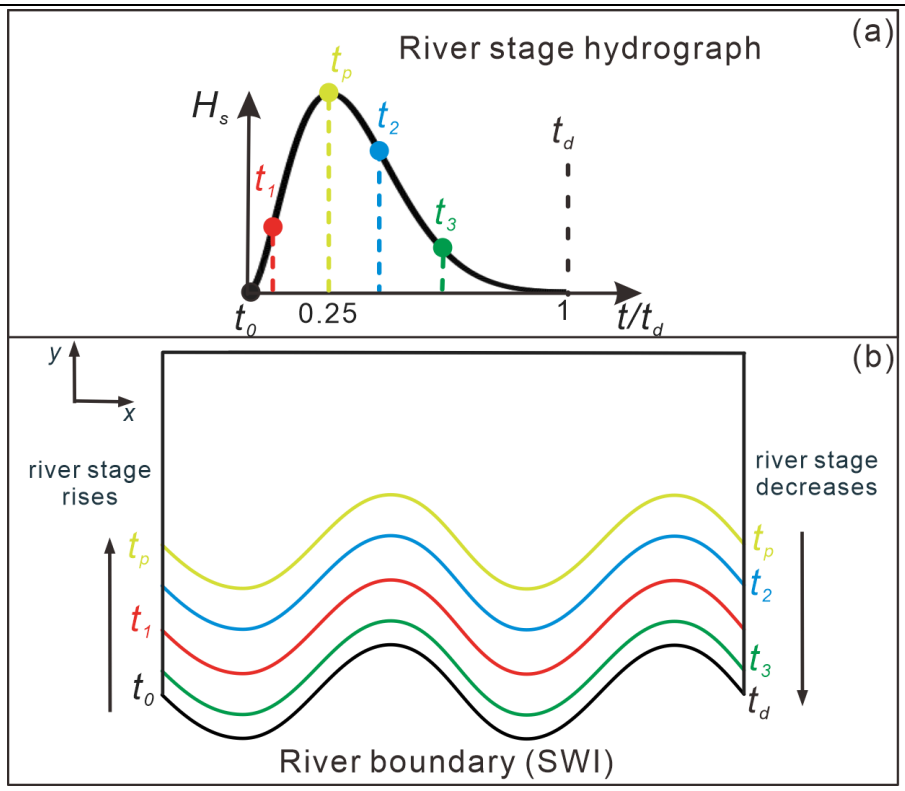

Figure 1. (a) River stage hydrograph during the flood event; (b) diagram showing displacement of SWI during the flood event. The colored SWIs in (b) correspond to the times of colored dots in (a). When the river stage increases, the river boundary migrates into the aquifer and recovers to its initial location as river stage decreases. The upward and downward arrow in Fig. 1b indicates the raising and decreasing of river stage, respectively.

2.2 Model parameterization, testing and scenarios

Hydraulic conditions used in our numerical modeling study are based on values from Gomez-Velez et al. (2017), who conducted a Monte Carlo analysis. They found that the dynamic variations of HEF and RTD are mainly determined by ambient groundwater flow and the ratio of aquifer hydraulic conductivity to the duration of the flood event (referred to as dimensionless constant $\Gamma_d = \frac{S_y \lambda^2}{0.5K(1+n_0)H_0 t_d}$, see Table 1 and Fig. S2, where S_y is specific yield [-]; λ is wave length of sinuous river; K is hydraulic conductivity [LT^{-1}]; n_0 is intensity of flood event [-] H_0 is base river stage [L]; t_d is

duration of flood event [T]).

After setting up the baseline model case with a vertical riverbank (δ = 90°), we compared our model results for that case with those obtained by Gomez-Velez et al. (2017) for (a) net HEF represented by $Q^*_{net,\,HZ}(t)$; (b) area of HZ, $A^{**}(t)$; (c) penetration of the HZ, $d^*(t)$ for Γ_d = 0.1, 1, 10 and 100, and found that our model simulated those cases with high accuracy (Fig. 2). Parameters $A^{**}(t)$ and $d^*(t)$ are based on modeling the transport of a conservative solute while $Q^*_{net,\,HZ}(t)$ is based on modeling water flow. Slight differences between our model and that of Gomez-Velez et al. (2017) might be due to the use of a much more refined mesh in this study as well as different length scales.

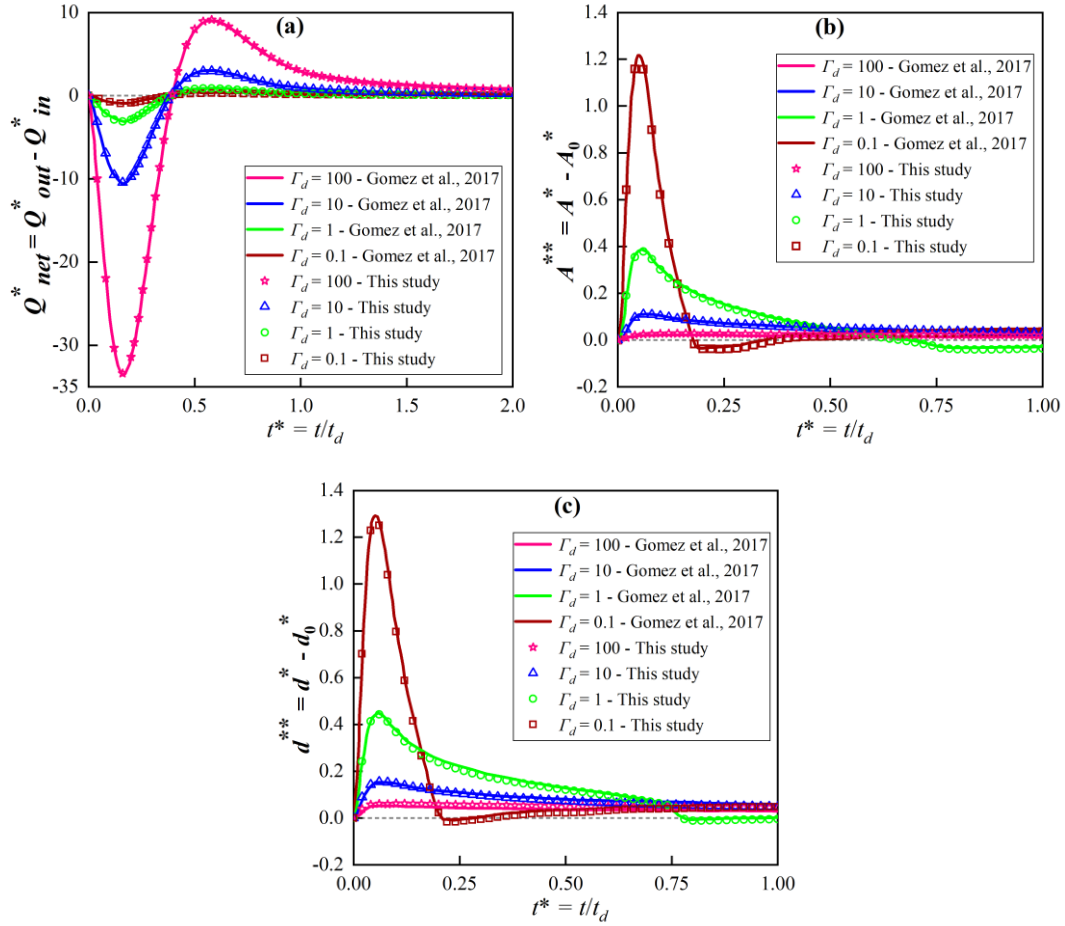

Figure 2. Comparison of results obtained in this study with those of Gomez et al. (2017) for the baseline case with a vertical river bank and variable Γ_d: (a) net hyporheic

exchange flux represented by $Q^*_{net,HZ}(t)$; (b) extent of the hyporheic zone $A^{**}(t)$ and (c) penetration distance $d^*(t)$ of the hyporheic zone into the alluvial valley. A more refined mesh and different length scales used in this study can explain slight variations between our model and that of Gomez et al. (2017). Information regarding model fits can be found in the SI.

To test, whether our assumption of considering a vertical SWI and using the DGM to characterize the migration of the SWI was appropriate, we compared the vertical 2-D model with a 1-D model coupled with the DGM. Detailed information on this comparison as well as validation results are listed in the SI in section S4. The results show that our approach is reasonable when simulating HEF in a sloping riverbank aquifer.

We then considered a series of riverbank scenarios where the bank slope angle ranged from $\delta = 90°$ (vertical riverbank) to 10° (nearly horizontal case) and Γ_d values ranged from 0.1 to 100, corresponding to aquifer hydraulic conductivity ranging from 480 to 0.048 m/d, indicating high to low transmissivity. Table 1 presents the parameters used in our numerical modeling study. The finite-element models proposed in this study were set up using the COMSOL Multiphysics (COMSOL) software. Eq. (S1), Eq. (S3) and Eq. (S6) were implemented by using customized a Partial Differential Equation (PDE) interface to include the Boussinessq equation, vertical integrated solute transport equation and equation for calculating residence (travel) time distributions (RTD), respectively. The model domain was discretized into about 0.5 million variably-sized triangular elements, with refinement imposed near the river boundary. Mesh-independent numerical solutions are achieved by limiting grid size (ΔL) to less than 0.2 m. Thus, the transverse and longitudinal Peclet numbers (calculated by $P_e = \Delta L/\alpha_L$ and $P_e = \Delta L/\alpha_T$, respectively) in both advection and diffusion dominated zones are less than 1, which is smaller than the upper limit of $P_e = 4$ to effectively avoid numerical oscillations and instabilities.

262 **Table 1**. Parameters and values used in our numerical model simulations.

Parameters	Value	Description
Constant model parameters		
S_y	0.3	Specific yield [-]
λ	40	River boundary wave length [L]
α	5	River boundary amplitude [L]
θ	0.3	Efficient porosity [-]
J_x	0.0025	Base groundwater gradient [-]
σ	1.14	River boundary sinuosity [-]
t_d	10	Duration of flood event [T]
n_d	0.25	Skewness of flood event [-]
t_p	$n_d t_d$	Time to peak river stage [T]
H_0	1	Base river stage [L]
n_0	1	Intensity of flood event [-]
α_L	2	Longitudinal dispersivity [L]
α_T	$0.1\alpha_L$	Transverse dispersivity [L]
Variable model parameters		
Γ_d	0.1 1 10 100	Dimensionless aquifer transmissivity [-]
δ	90 70 50 20 10	Bank slope angle [°]

263

264 Similar to Gomez-Velez et al. (2017), we evaluate the impact of bank slope by
265 comparing the net hyporheic exchange flux ($Q^*_{net,\ HZ}$ (t)), area of HZ (A^{**}(t)),
266 penetration distance of the HZ (d^{**}(t)) and RTD (μ_r^*($\mathbf{x}$, t)) between vertical and sloping
267 river bank models. A detailed definition of these variables is provided in the SI (section
268 S5).
269

3. Results

3.1 Effect of bank slope on hyporheic exchange flow and HZ extent

3.1.1 Hyporheic exchange flow

The flow field (velocity magnitude and direction) and net HEF ($Q^*_{net,\ HZ}\ (t)$) changed dynamically during and after the simulated flood event. Fig. 3a – 3d show the evolution of net HEF for different aquifer transmissivity (Γ_d) and bank slope angle (δ) condition. Snapshots of the flow field and the boundary of the HZ area (isolines of $C(\mathbf{x}, t) = 0.5$ as concentration of a conservative solute) for different δ conditions at different times (pink dots in Fig. 3a) for $\Gamma_d = 1$ are shown in Fig. 4a - 4f.

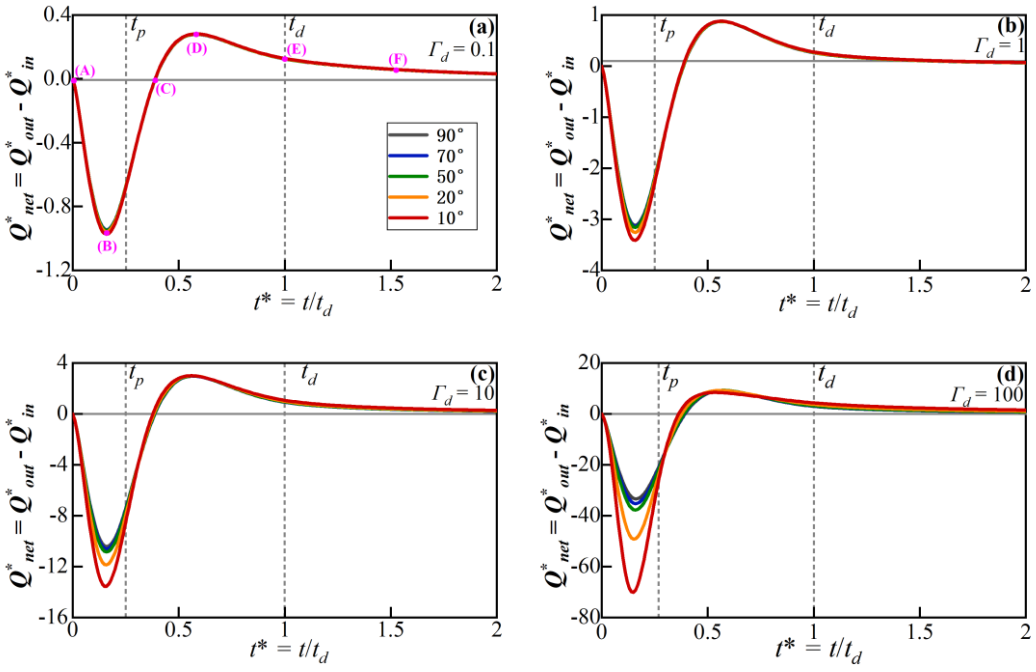

Figure 3. Temporal evolution of dimensionless net HEF ($Q^*_{net,\ HZ}\ (t)$) for four different aquifer transmissivity values (represented by Γ_d) and bank slopes angles (δ, from 10-90 degrees). Time-to-peak flood (t_p) and flood duration (t_d) are marked by vertical dashed lines. Pink dots in (a) marked by (A) - (F) correspond to the snapshots of the flow field shown in Fig. 4. A negative flux value here represents water flow from river to aquifer.

Note that Γ_d negatively correlates with the transmissivity of aquifer.

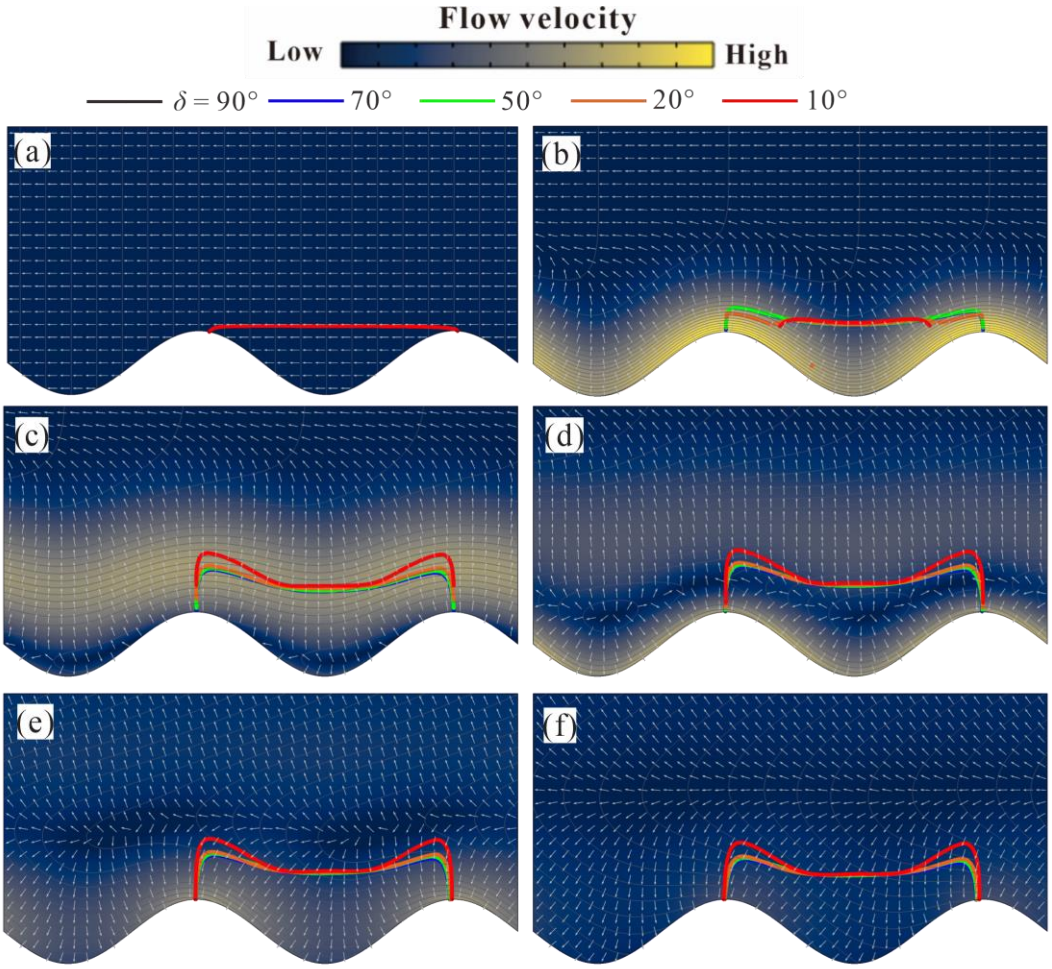

Figure 4. Plan view of the river channel and aquifer showing the temporal evolution of the alluvial flow field and spatial extent of the HZ. (a)-(e) are snapshots of the flow field at different time steps during the simulated event (pink dots in Fig. 3a). Colored surfaces represent the magnitude of the Darcy flux vector (blue is low and yellow is high) and white isolines the dimensionless hydraulic head. Bold colored lines correspond to the HZ extent for different bank slope conditions.

Before the flood event ($t = 0$), steady-state base flow conditions are assumed, as shown in Fig. 4a. The inflow and outflow (along the upstream and downstream meander bend, respectively) are in balance. The bank slope has no effect on the HZ boundaries before the flood event.

Before peak river stage of the flood event is reached ($0 < t < 0.25t_d$), the onset of the flood event is indicated by the rising river stage and forces the river to infiltrate into the aquifer along the SWI (negative values of $Q^*_{net,\,HZ}(t)$ in Fig. 3), resulting in the expansion of the HZ as shown in Fig. 4b. The influx of river water into the HZ ($-Q^*_{net,\,HZ}(t)$) reaches its maximum before the time-to-peak river stage ($t = 0.25t_d$) because the pressure wave propagates into the aquifer and decreases the head gradient between the river and the connected aquifer. For higher transmissivity aquifers (Lower Γ_d values in Fig. 3), bank slope has a reduced impact on net outflux as the fast propagation of the pressure wave results in the hydraulic head near the SWI to be very similar. Among different aquifer transmissivity conditions. As aquifer transmissivity decreases, the ability of the aquifer to transmit the pressure wave becomes limited, and the interaction flux is dominated by the location (displacement) of the SWI and the river stage. On the other hand, a smaller slope angle induces a longer displacement of the SWI ($M(t)$) away from the river, where the groundwater head adjacent to the SWI is always relatively high (i.e., the head in base flow condition). This, consequently, leads to a larger head gradient near the SWI as well as larger dimensionless net fluxes under increasing Γ_d conditions as shown in Fig. 3.

The maximum dimensionless flux ratios $Q^*_{max,\,var} = Q^*_{max,\,s} / Q^*_{max,\,v}$ of sloping ($\delta < 90°$, $Q^*_{max,\,s}$) vs vertical ($\delta = 90°$, $Q^*_{max,\,v}$) riverbank cases are shown in Fig. 5, which indicates the deviation in predicting peak net flux when neglecting the slope of the riverbank. The bank slope is found to increase infiltration by up to 120% ($Q^*_{max,\,var} \approx 2.2$) for $\Gamma_d = 100$ with $\delta = 10°$ while for larger slope angles or higher hydraulic transmissivities the dimensionless infiltration gradually decreases.

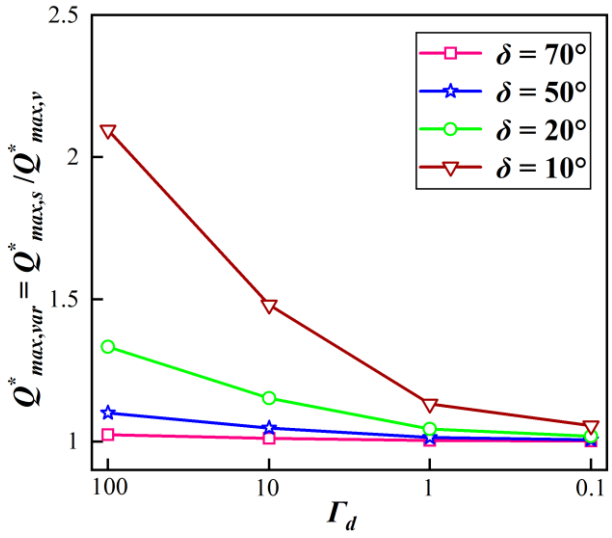

Figure 5. Ratio of maximum net flux for slope to no-slope (vertical river bank) conditions $Q^*_{max,var} = Q^*_{max,s}/Q^*_{max,v}$ for four aquifer transmissivities and slope angles. Note that Γ_d negatively correlates with aquifer transmissivity.

As the river stage decreases after t_p, the head gradient near the SWI gradually reverses and the net outflux starts increasing (the river is gaining water) as shown in Fig. 3. This is associated with the river stage declining below the groundwater level (see Fig. 4c - 4f). For the lowest hydraulic transmissivity condition (Γ_d = 100), bank slope can slightly extend the time required for the system to recover to initial conditions after t_p but in general, the response of the net outflux to bank slope is negligible when compared to that of the influx. Eventually, the net flux converges to zero, which indicates the flow field within the aquifer recovers to the initial conditions. The bank slope has no impact on the HEF after the duration of flood event.

3.1.2 Patterns of hyporheic area and penetration distance

Fig. 6 and Fig. 7 show the temporal evolution of the dimensionless HZ area ($A^{**}(t)$) and penetration distance ($d^{**}(t)$) into the alluvial valley relative to the initial condition for varying aquifer transmissivity (Γ_d) and slope angles.

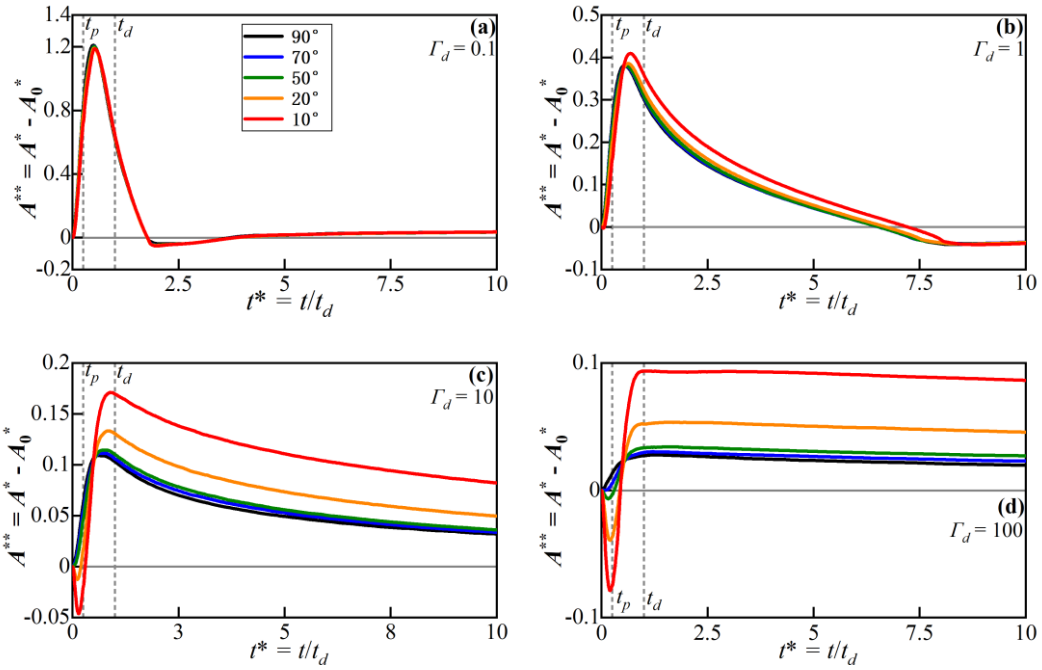

Figure 6. Temporal evolution of dimensionless HZ area for different values of Γ_d and δ (colored lines). Time-to-peak (t_p) and flood duration (t_d) are marked by vertical dashed lines.

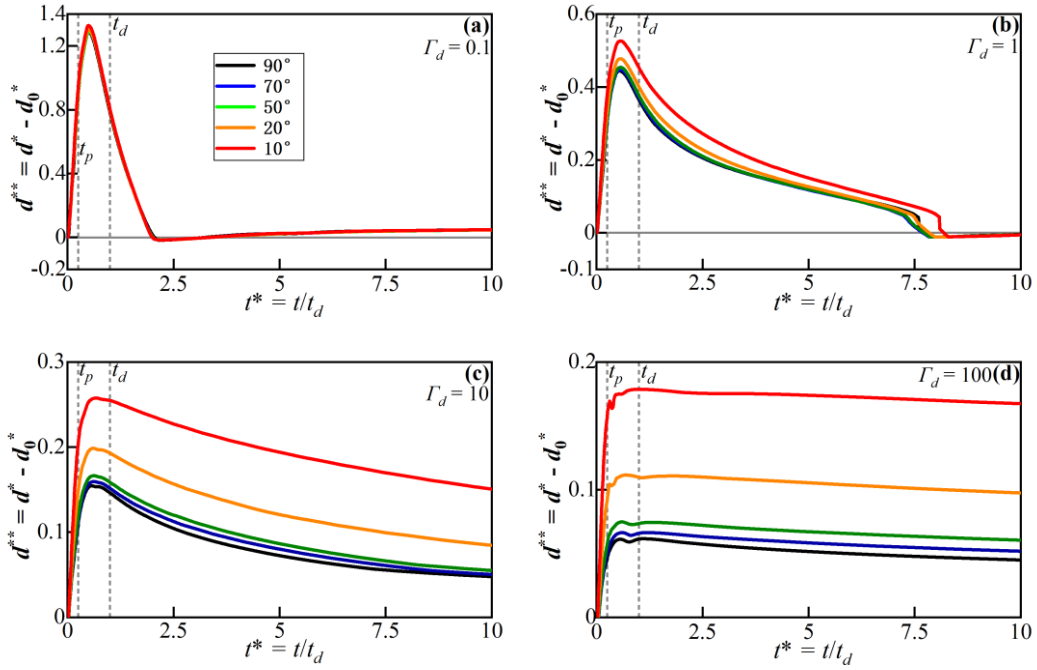

Figure 7. Temporal evolution of dimensionless HZ penetration distance into the alluvial valley (d^{**}) for different values of Γ_d and δ (color lines). Time-to-peak (t_p) and flood duration (t_d) are marked by vertical dashed lines.

For vertical banks (δ = 90°, black lines in Fig. 6), the HZ area increases synchronously with the river stage ($t < t_p$). After the peak time of the flood event ($t > t_p$), the HZ area continues to extend as river water still recharges the aquifer. After the flood event ($t > t_d$), the river water that was stored in the aquifer ($C(\mathbf{x}, t) > 0$) slowly discharges back into the river channel. Thus, the HZ area and penetration distance gradually rebound to initial conditions.

Under sloping riverbank conditions, the riverbank will at times be submerged by the rising river stage. Fig. 6a and 7a show that the effects of bank slope on HZ area ($A^{**}(t)$ in Fig. 6) and penetration distance ($d^{**}(t)$ in Fig. 7) are almost counteracted by the high transmissivity of the aquifer and the influence of bank slope was negligible. At the beginning of the flood event, Fig. 6b – 6d show that for conditions with smaller sloping angle, HZ area can be less than zero (HZ at these times are smaller than the initial condition). This is due to the fact that the movement of the SWI during a rising river stage towards the alluvial valley will submerge parts that were previously unsaturated as the aquifer with low transmissivity will propagate water more slowly. As aquifer transmissivity decreases from Fig. 6b – 6d, the relative HZ area remains negative for a longer time for smaller bank slopes. This indicates that bank slope has a more pronounced effect on HZ extent in cases where aquifer transmissivity is large as a low-transmissivity aquifer takes more time to propagate infiltrating river water.

After about half the flood duration ($t > 0.5t_d$), the HZ area (A^{**}) becomes positive in all scenarios as the model domain previously submerged during the flood event re-emerges. As aquifer transmissivity decreases (Fig. 6a – 6d and Fig. 7a – 7d), the impact of bank slope gradually increases especially in low aquifer transmissivity conditions, where smaller bank slope can increase the peak values of area and penetration distance, and delay the arrival time-to-peak value of the relative HZ area. After the flood event ($t > t_d$), the effect of bank slope is counteracted by the higher aquifer transmissivity and only lower transmissivities have a significant impact on the HZ resulting in larger $A^{**}(t)$

and $d^{**}(t)$ as shown in Fig. 6b – 6d and Fig. 7b – 7d. For low transmissivity scenarios, the bank slope can increase the peak area and penetration of HZ by almost 200%.

3.2 Spatiotemporal evolution of mean residence time distribution

The evolution of spatiotemporal patterns of mean RTD (i.e., travel time of river water in aquifer) is a useful evaluation method for identifying the dynamic variation of aging and rejuvenation of hyporheic water. Here we use the mean RT ratio between a sloping model and a vertical model $\mu_r^*(\mathbf{x}, t) = \log_{10}(\mu_{\tau\text{-}S}(\mathbf{x}, t)/\mu_{\tau\text{-}V}(\mathbf{x}, 0))$ to evaluate the influence of bank slope on the prediction of RTD for a given location and time. Fig. 8 presents RTDs for the initial condition, where $\mu_{\tau 0\text{-max}}$ is the maximum RT in the domain. It can be seen that the isolines representing the RT are almost horizontal in the area extending from the river but RT near the upstream river bend is smaller than downstream because the initial flow direction is towards the negative direction of the x axis. Notably, $\mu(\mathbf{x}, 0)$ grows almost exponentially as y increases, and a positive correlation to Γ_d at a given location is observed.

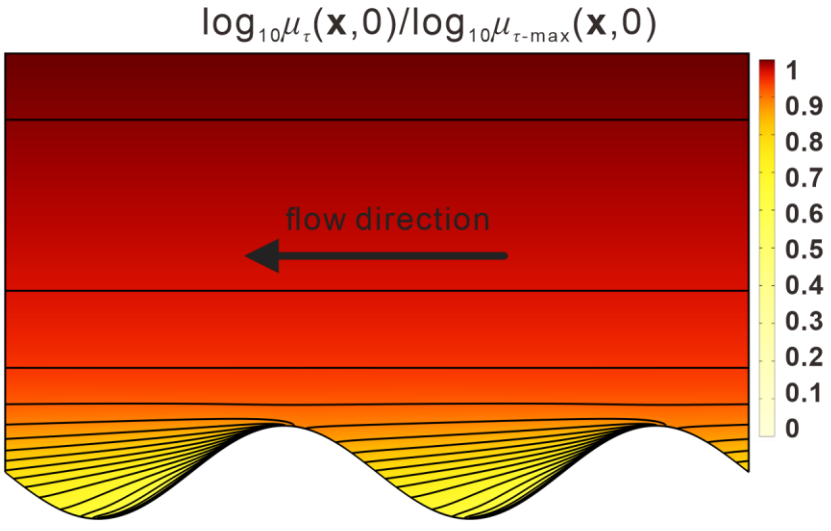

Figure 8. Relative mean residence time distributions [-] for baseline flow conditions (no bank slope), which are represented by $\log_{10}\mu_\tau(\mathbf{x}, 0)/\log_{10}\mu_{\tau\text{-max}}(\mathbf{x}, 0)$ to show the distribution pattern. The value of the contour lines grows exponentially with the distance from the river meander.

Fig. 9 - 12 present five snapshots of μ_r^* for different bank slope angles and different aquifer transmissivity aquifers (Γ_d = 0.1, 1, 10 and 100, respectively) . The five snapshots represent the rising limb of the flood event (t/t_d = 0.1), the peak of the flood event (t/t_d = 0.25), the falling limb of the flood event (t/t_d = 0.5) and a time after the flood event (t/t_d = 1, 2.5 and 10). The RT differences between sloping and vertical riverbank models are within 12.2% in the white-colored areas (-0.05 < μ_r^* < 0.05) of Fig. 9 - 12, which indicates a minor effect of bank slope on RTD. The colored areas in Fig. 9 – 12 indicate model results where neglecting bank slope will lead to overestimated (μ_r^* < -0.05) or underestimated (μ_r^* > 0.05) of residence (travel) time.

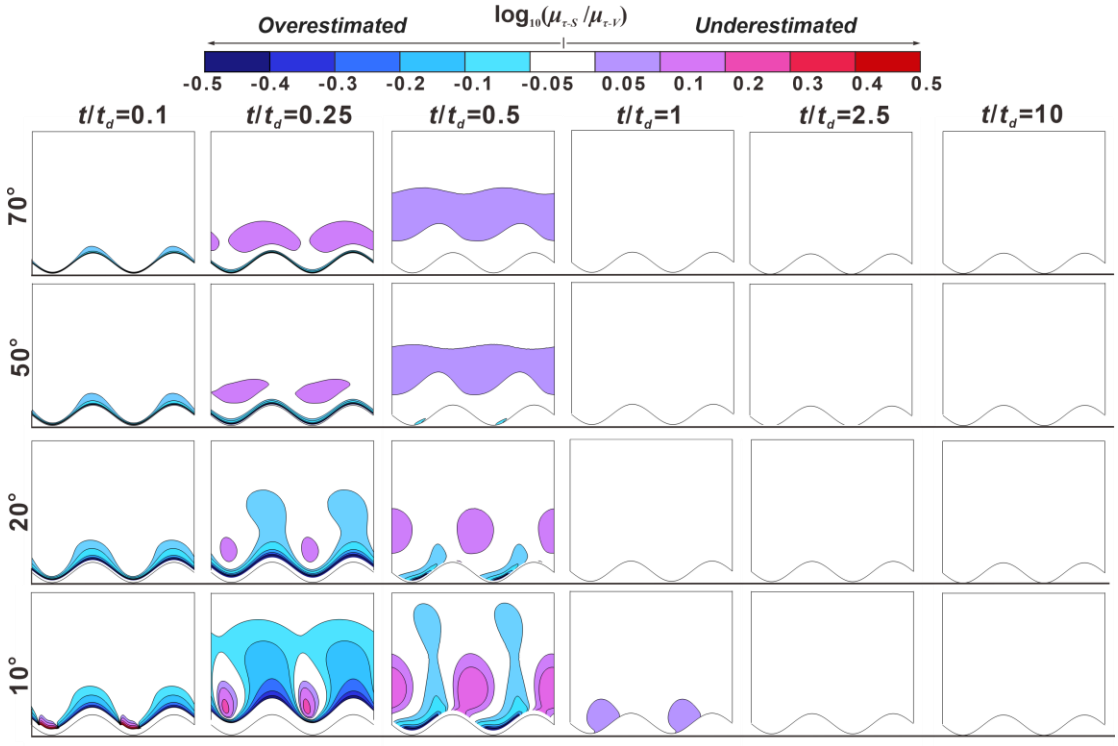

Figure 9. Five snapshots for the RTD ratio ($\mu_r^*(\mathbf{x}, t) = \mu_{r\text{-}S}^*(\mathbf{x}, t)/ \mu_{r\text{-}V}^*(\mathbf{x}, t)$) between sloping ($\mu_{r\text{-}S}^*(\mathbf{x}, t)$) and vertical riverbank conditions ($\mu_{r\text{-}V}^*(\mathbf{x}, t)$) at different times t/t_d as a function of δ for Γ_d = 0.1.The horizontal lines beneath each figure are the reference lines to show the initial location of the peak point of the point bar. The lower sinuous lines at the reference lines are the initial SWIs. The colored areas indicate where the bank slopes have significant impact on RT (difference in RT between sloping and

vertical model larger than 12.2%) and residence (travel) times of river water in the aquifer would be overestimated or underestimated.

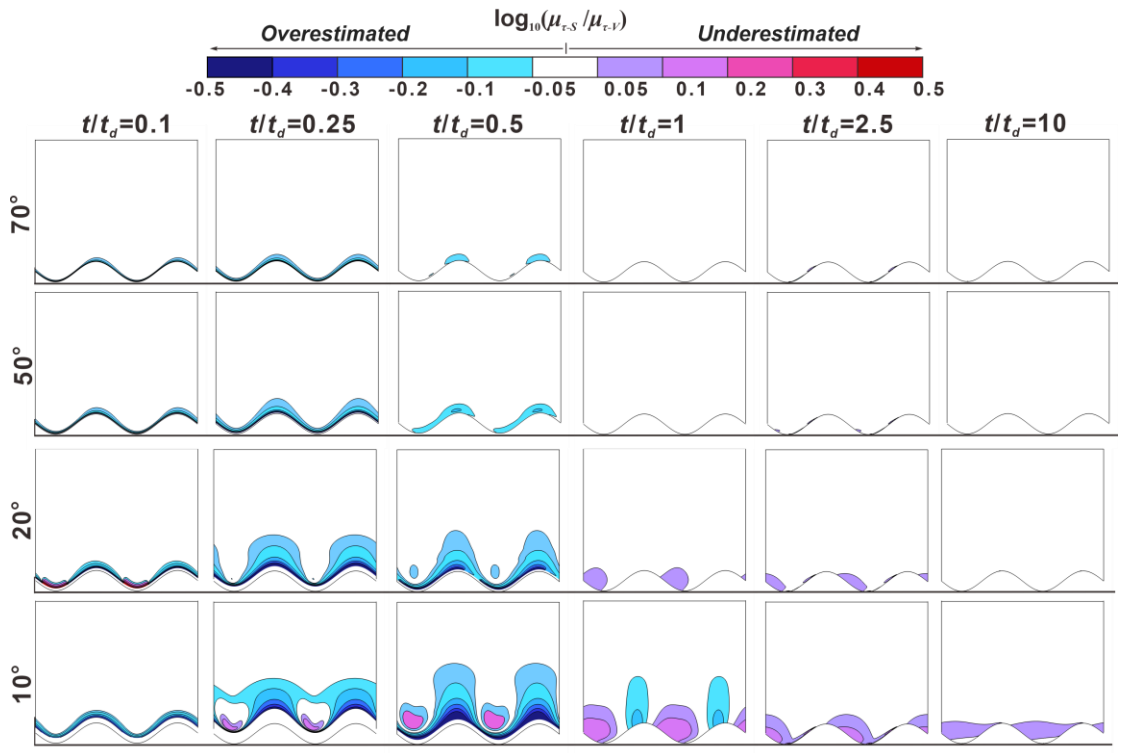

Figure 10. Five snapshots for the RTD ratio ($\mu_r^*(\mathbf{x}, t) = \mu_{r\text{-}S}^*(\mathbf{x}, t)/\ \mu_{r\text{-}V}^*(\mathbf{x}, t)$) between sloping ($\mu_{r\text{-}S}^*(\mathbf{x}, t)$) and vertical riverbank conditions ($\mu_{r\text{-}V}^*(\mathbf{x}, t)$) at different times t/t_d as a function of δ for $\Gamma_d = 1$.The horizontal lines beneath each figure are the reference lines to show the initial location of the peak point of the point bar. The lower sinuous lines at the reference lines are the initial SWIs. The colored areas indicate where the bank slopes have significant impact on RT (difference in RT between sloping and vertical model larger than 12.2%) and residence (travel) times of river water in the aquifer would be overestimated or underestimated

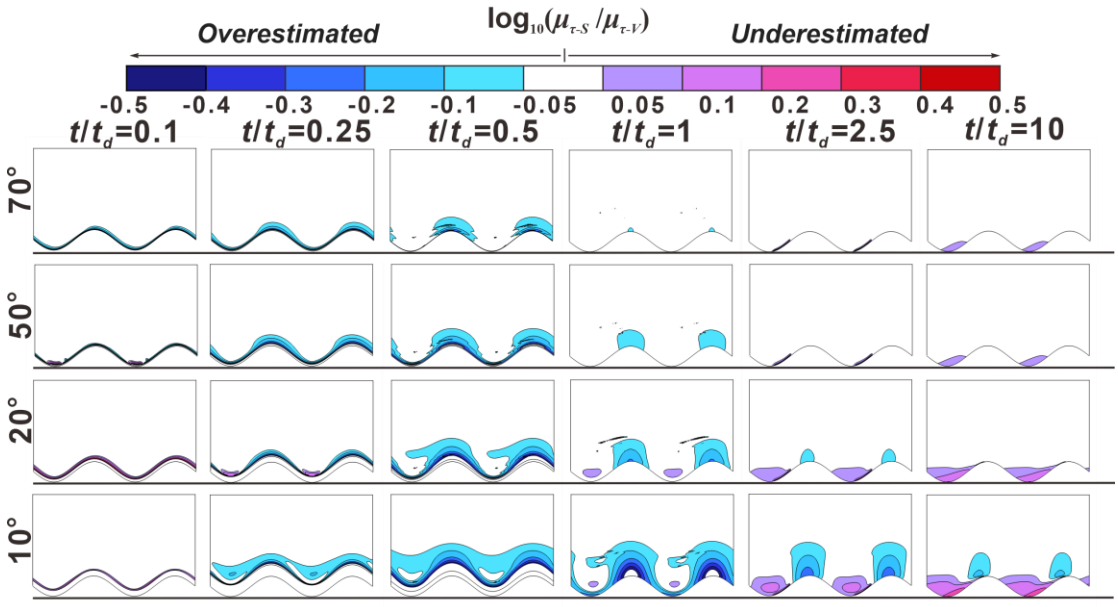

433

434 **Figure 11.** Five snapshots for the RTD ratio ($\mu_r^*(\mathbf{x}, t) = \mu_{r\text{-}S}^*(\mathbf{x}, t)/\ \mu_{r\text{-}V}^*(\mathbf{x}, t)$) between
435 sloping ($\mu_{r\text{-}S}^*(\mathbf{x}, t)$) and vertical riverbank conditions ($\mu_{r\text{-}V}^*(\mathbf{x}, t)$) at different times t/t_d
436 as a function of δ for $\Gamma_d = 10$.The horizontal lines beneath each figure are the reference
437 lines to show the initial location of the peak point of the point bar. The lower sinuous
438 lines at the reference lines are the initial SWIs. The colored areas indicate where the
439 bank slopes have significant impact on RT (difference in RT between sloping and
440 vertical model larger than 12.2%) and residence (travel) times of river water in the
441 aquifer would be overestimated or underestimated
442

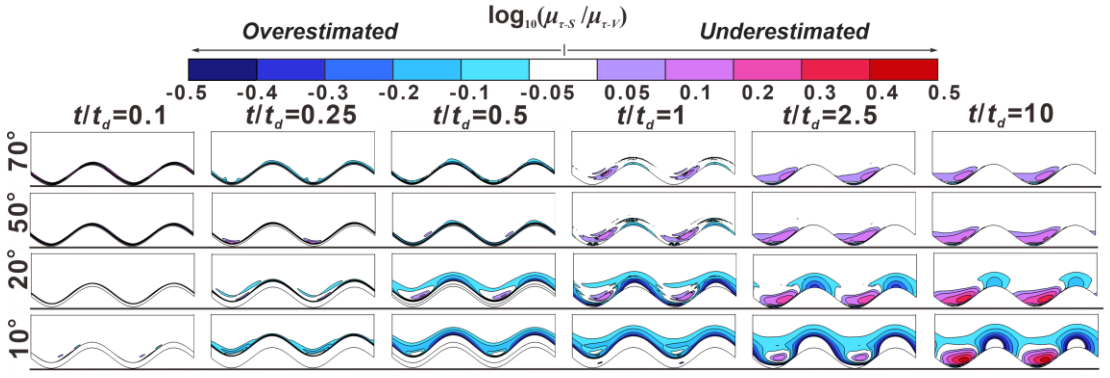

443

444 **Figure 12.** Five snapshots for the RTD ratio ($\mu_r^*(\mathbf{x}, t) = \mu_{r\text{-}S}^*(\mathbf{x}, t)/\ \mu_{r\text{-}V}^*(\mathbf{x}, t)$) between
445 sloping ($\mu_{r\text{-}S}^*(\mathbf{x}, t)$) and vertical riverbank conditions ($\mu_{r\text{-}V}^*(\mathbf{x}, t)$) at different times t/t_d
446 as a function of δ for $\Gamma_d = 100$.The horizontal lines beneath each figure are the reference

447 lines to show the initial location of the peak point of the point bar. The lower sinuous
448 lines at the reference lines are the initial SWIs. The colored areas indicate where the
449 bank slopes have significant impact on RT (difference in RT between sloping and
450 vertical model larger than 12.2%) and residence (travel) times of river water in the
451 aquifer would be overestimated or underestimated
452
453 At t/t_d = 0.1, a smaller bank slope can lead to shorter travel time of river water in
454 the aquifer (negative values of μ_r^*) near the SWI compared to the vertical riverbank
455 scenario. The area of shorter travel time caused by bank slope was positively related to
456 aquifer transmissivity. The effect of bank slope is small for Γ_d = 10 and 100 because the
457 groundwater mound (the raised groundwater stage) piles up around the river boundary,
458 but that small area extended deeper into the alluvial valley for smaller slope angles.
459 Due to the scattered and nested flow paths near the cut bank and point bar, respectively,
460 the area of negative value of μ_r^* at the cut bank of SWI is larger than that at the point
461 bar. The change of flow direction near the point bar leads to a prolonged flow path for
462 the water in the river as well as to forced groundwater mixing with the slightly older
463 water (as shown in Fig.8 that the water was more aged in y direction compared to $-x$
464 direction in the point bar). This effect was amplified with decreasing bank slope angle,
465 but it is only statistically significant ($\mu_r^* < -0.05$ or $\mu_r^* > 0.05$) when $\delta = 10°$ at t/t_d =
466 0.1.
467 At the time of peak flood (t/t_d = 0.25), the river still infiltrates into the aquifer.
468 For Γ_d = 0.1, results of μ_r^* in Fig. 9 show that bank slope can lead to both overestimated
469 and underestimated RT area. Both magnitude of relative RT (μ_r^*) and associated area
470 increase with decreasing slope due to the longer travel distance of river water into the
471 aquifer. As the slope angle decreases, the underestimated travel time area was located
472 closer to the peak of the cutbank. The impact of bank slope on RTD for Γ_d = 1 was
473 rather similar in its pattern compared to Γ_d = 0.1, but the degree of that impact was
474 reduced. For Γ_d = 10 and 100, only overestimated travel time area can be seen near the

river bank with a smaller area of impact compared to smaller Γ_d conditions, because the groundwater has not sufficiently propagated into the aquifer due to lower transmissivity.

At $t/t_d = 0.5$, part of the aquifer that was submerged at $t/t_d = 0.25$ reemerges due to the decline in river stage. In most cases, smaller bank slopes can lead to wider reemergence of the aquifer, which therefore results in overestimated travel time area near the river boundary; however, this was not the case for $\Gamma_d = 0.1$ where bank slope can both lead to overestimated and underestimated travel time area. Furthermore, compared to when $t/t_d = 0.25$, the impact of bank slope becomes weaker for $\Gamma_d = 0.1$, but more relevant for the larger Γ_d values.

After the flood event ($t/t_d > 1$), the influence of bank slope on travel time is nearly eliminated for $\Gamma_d = 0.1$ and 1 due to the high aquifer transmissivity. However, for aquifers with lower transmissivity ($\Gamma_d = 10$ and 100), bank slope still has a significant effect on RT at $t/t_d = 10$ and leads to underestimated and overestimated RT area near the point bar and the cut bank, respectively

Overall, Fig. 9-12 indicate that the time when bank slope was relevant in predicting RT (travel time of groundwater in aquifer) was determined by the transmissivity of aquifer. For higher transmissivity aquifer, the impact of bank slope on the prediction of groundwater travel time cannot be neglected during the flood event ($0 < t < t_d$), but that impact will be eliminated after flood event due to the quickly recovery of aquifer to the base condition. For lower transmissivity aquifer, bank slope plays an important role on groundwater travel time after the half time of flood event ($t > 0.5*t_d$) and has a more lasting influence on aquifer RT, as more time is required to recover to initial condition for lower transmissivity aquifer.

3.3 Relative flux-weighted residence time

Fig. 13 shows the evolution of the flux-weighted relative RT $\mu^*_{out}(x, t) = \mathbf{n}\cdot Q^*_{out}(x, t)\log_{10}(\mu_\tau(x, t)/\mu_\tau(x, 0))$ for different slopes and aquifer transmissivities. $M^*_{out}(x, t)$ represents the difference in flux-weighted RT of the water discharged into the river

compared to the initial condition. At the start of the flood event, there is no μ^*_{out} as river water infiltrates the aquifer. Following the decline in river stage, the aquifer begins to discharge the mixed water with different RT back into the river (see Fig. 4c).

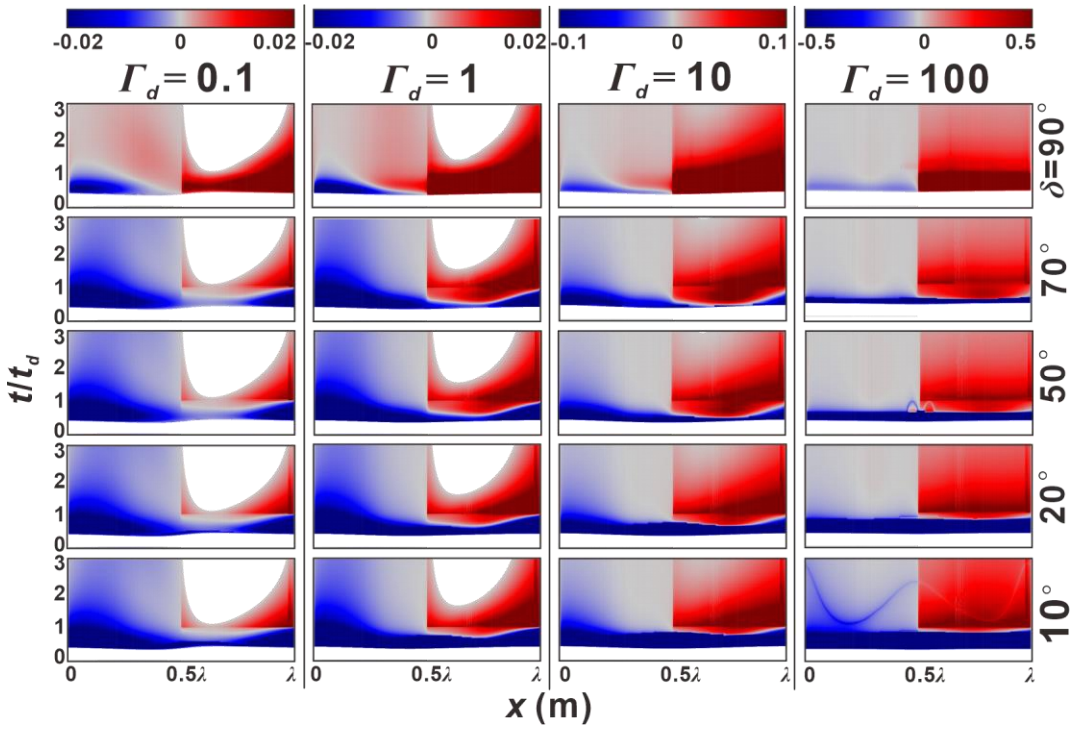

Figure 13. Temporal evolution of flux-weighted ratios of RT to the RT for baseline conditions ($\mu^*_{out}(x, t) = \mathbf{n}\cdot Q^*_{out}(x, t)\log_{10}(\mu_\tau(x, t)/\mu_\tau(x, 0))$) along the river meander as a function of δ and Γ_d. $\mu^*_{out}(x, t)$ indicates the difference of flux weighted water RT (travel time) that the aquifer discharges into river compared to the initial condition.

For vertical riverbank conditions ($\delta = 90°$, top row in Fig. 13), upstream ($0.5\lambda < x < \lambda$) and downstream ($0 < x < 0.5\lambda$) boundaries of the meander bend discharge older and younger water, respectively. The rejuvenated or aged waters that represent shorter and longer travel times compared to the baseline condition, respectively, were mostly discharged before the flood event ($t/t_d < 1$) due to the greater outflux as shown in Fig. 3a. It also can be seen that water was aged along the upstream bend compared to the more rejuvenated water along the downstream bend. After the flood event, μ^*_{out} gradually disappears along the upstream meander (blank areas) for $\Gamma_d = 0.1$ and 1,

because the flow fields were recovering to baseline conditions. Therefore, the upstream meander gradually becomes the inflow boundary.

For cases with lower values of Γ_d (left columns in Fig. 13), μ^*_{out} reaches equilibrium earlier compared to cases with higher Γ_d . As δ the increased impact of bank slope causes μ^*_{out} to gradually decrease the travel time of the outflowing water during the flood event. For larger Γ_d, μ^*_{out} was totally dominated by rejuvenated water during the flood event. Furthermore, the stronger impact of smaller bank slope angles can both extend the time over which and increase the magnitude with which younger water was discharging along the downstream meander.

4. Discussion

4.1 Why we should account for bank slope

Tilted riverbanks are common in nature and caused by erosion and bank collapse, as has been observed at multiple scales (Zingg, 1940). Previous studies have shown that bank erosion is stronger where the river planimetry is more sinuous, river stage varies more frequently, or where the riverbank has larger sloping angles, ultimately leading to a flatter bank (Zingg. 1940; Hagorty et al., 1995; Mayor et al., 2008; Puttock et al., 2013). Yet, the impact of riverbank geometry and in particular bank slope on sinuosity-driven lateral hyporheic exchange was ignored in most previous studies. Our results clearly indicate that HZ characteristics (HEF, area and penetration distance of HZ into alluvial valley) can be underestimated along a meandering river depending on bank slope conditions.

We show that not accounting for bank slope and river sinuosity can lead to an underestimation of the infiltration rate of water from the river to the alluvial aquifer (by up to 120%), as well as the area and penetration distance. This effect is more pronounced for smaller bank slope angles (Fig 5), which can be more likely found in

lowland streams (Laubel et al., 2003), especially in areas with extensive cattle grazing streamside (Trimble, 1994).

Doble et al. (2012), Siergieiev et al. (2015) and Liang et al. (2018), assessed the influence of bank slope on HEF using a vertical cross-sectional profile. Siergieiev et al. (2015) found that the impact of bank slope on HEF was proportional to the hydraulic conductivity of the aquifer. However, we argue here that bank slope is more relevant in rivers connected to aquifers with low hydraulic transmissivity (high hydraulic conductivity or low specific yield). Furthermore, we show (Fig. 14 as example) that using only one cross-sectional river profile perpendicular to the river axis does not capture the effect of river sinuosity on HEF as bank storage decreases from point bar to cut bank. This indicates that the accuracy of bank storage estimates can be improved by including river sinuosity, which has often been omitted in the past. In a meandering river with variable bank slope, river geometry thus has a sizable effect on bank storage evolution and HEF, and should be included in any scenarios.

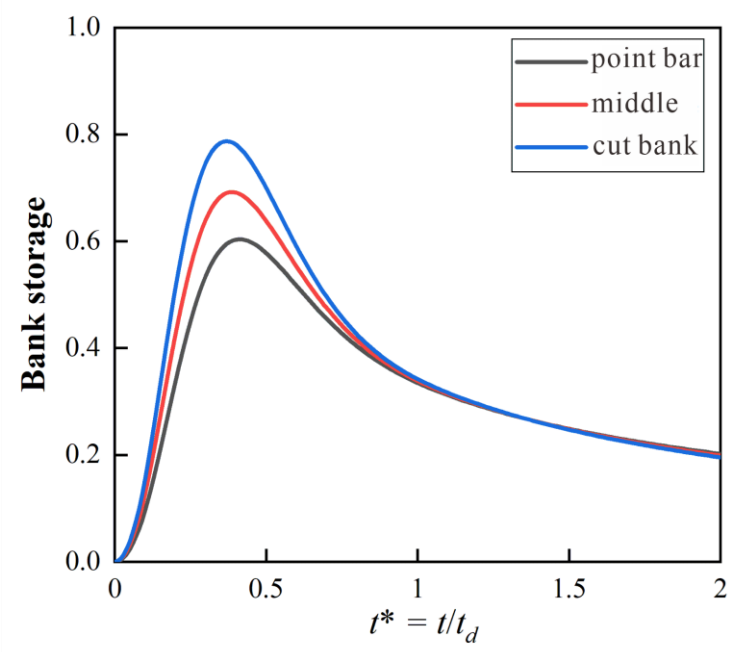

Figure 14. Bank storage versus time for $\Gamma_d = 1$ and $\delta = 90°$ condition at: the peak of point bar ($x = 0$); middle ($x = 0.25\lambda$); peak of cut bank ($x = 0.25\lambda$). Dimensionless bank

storage was calculated by $\frac{\int_{Y(x,t)}^{Y(x,t)+4\lambda}[h-z_b-H_0]\mathrm{d}y}{\lambda H_p}$.

4.2 Implications of bank slope on biogeochemical reactions

Residence time distributions of river water in the alluvial aquifer have been used to evaluate the potential of biogeochemical reactions by comparing the RT with biogeochemical timescales (BTS) for given solutes (Boano et al., 2010b; Gomez-Velez et al., 2012). Locations where the ratio of RT to BTS is small indicate a high reaction potential for that chemical species. It has been documented that the BTS for dissolved organic matters (DOC) is site-dependent and can vary over ten orders of magnitude (10^{-1} – 10^{9} d) (Hunter et al., 1998), while BTS for oxygen and nitrite have been found to vary over eight orders of magnitude (10^{-2} – 10^{6} d) (Gomez-Velez et al., 2012). Here, we compare the RTD within these two BTS ranges for vertical and sloping riverbank condition (δ = 10°) at the peak time of the flood event (t/t_p = 0.25) for different aquifer transmissivity conditions, and show the zonation of residence times by using a BTS range of 10^{-1} – 10^{6} d (Fig. 15).

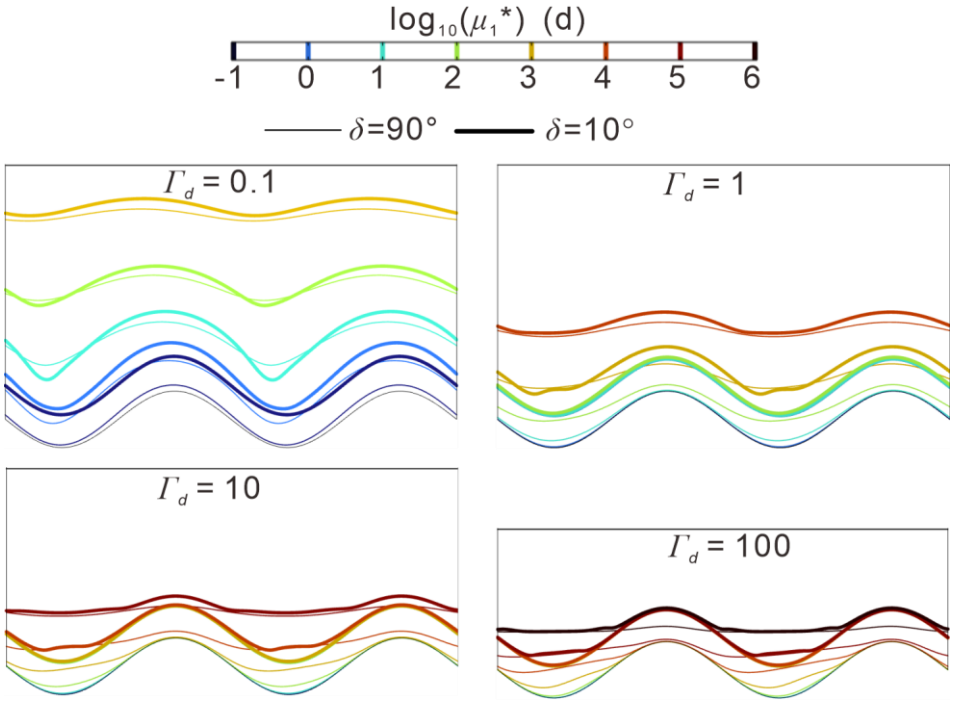

Figure 15. Zonation of biogeochemical timescales (BTS, range of 10^{-1} – 10^{6}) for common HZ constituents such as DOC, oxygen or nitrate for different aquifer transmissivities at $t/t_p = 0.25$. thick and thin lines indicate the comparison of vertical vs sloping riverbank ($\delta = 10°$) conditions, while the different colors indicate the different exponents.

Fig. 15 indicates that neglecting bank slope will impact the prediction of reaction potentials during the hyporheic exchange process, especially for locations with short time scales. For sloping bank conditions, the reaction hot spots (areas) expanded into the aquifer, identical to the overestimated areas in Fig. 9 to Fig. 12. Note that we did not aim to include specific reaction models in our study but used RTD as an indicator for various biogeochemical reactions in the aquifer.

The Impact of bank slope on RT is basically controlled by aquifer transmissivity. When aquifer transmissivity increases, the impact of bank slope appears to be more pronounced when the river stage rises during a flood event. For decreasing aquifer transmissivity, bank slope seems more relevant for RTD after the flood event and its impact is more long-lasting. Bank slope could result in longer (near the point bar) or shorter (near the cut bank) pore water travel times throughout the flood event. This means that point bars with bank slopes are more favorable for removing dissolved organic carbon and for nitrification while cut banks with bank slope may have adverse effects on the groundwater quality near rivers. As such, an analysis of residence time distributions can provide valuable information on whether and where riverbank slope can induce biogeochemical hotspots and hot moments and help guide choices to be made in biogeochemical field surveys regarding location and sampling time under dynamic river stage conditions, especially when the connected aquifers have low hydraulic transmissivity.

606 **4.3 Advantages and limitations of using a reduced 2-D model**

607 In this study, we propose a parsimonious reduced-order, idealized horizontal 2-D
608 model that simplifies the variation of the river-aquifer interface by using the moving
609 boundary method to depict the displacement of the SWI along a sloping riverbank. An
610 advantage of this approach is reduced model complexity as compared to a three-
611 dimensional model, which greatly reduces time and data requirements during model
612 building and computational demand during the simulation of HEF and especially
613 residence time distributions. Thus, our reduced-order model acts as a first step to gain
614 insight into the patterns of hyporheic exchange, riverbank storage and RTD in settings
615 with more complex riverbank morphology and dynamic forcing. Future efforts should
616 be focused on optimizing the computational method applied here and on including more
617 detailed morphology and hydrodynamic characteristics.

618 In our simulations we assume a constant bank slope angle along the entire
619 meandering river while natural riverbanks often change their slope angle from reach to
620 reach as well as with time. This variability could lead to more complex SWI travel
621 distances and residence time distributions and new conceptualizations that account for
622 the contribution of bank slope on time varying RTD and HZ extent are needed. In our
623 simulations we tested the model using a range of aquifer hydraulic conductivities.
624 Although hydraulic conductivity (or transmissivity) is a critical parameter in the
625 quantification of exchange fluxes and RTD between the two systems under varying
626 slope conditions, other parameters such as valley water head fluctuation, water
627 abstraction e.g. for agriculture or drinking water supply, peak flood event characteristics
628 or larger scale groundwater head fluctuation, e.g., due to changing groundwater
629 recharge in the context of changing rainfall patterns have not been considered here but
630 might also impact HZ extent, RTD and river-aquifer exchange flux. For example, valley
631 water head fluctuation and water abstraction in the aquifer will lead to a lower
632 groundwater table, increasing the hydraulic gradient between river and aquifer. This

will lead to the formation of a larger HZ area as well as longer travel distances and times of river water in the aquifer. Thus, reducing the slope of the river bank could reduce the infiltration of polluted river water into the riparian aquifer.

The current study assumes a perennial stream and unconfined (phreatic) conditions in the connected aquifer as well as changing hydraulic gradients leading to gaining and loosing conditions in the river. Where there is no hydraulic gradient between river and aquifer, no large-scale infiltration of river water into the riverbanks will occur, while local turbulent flow (e.g., due to obstacles in the river channel) might lead to localized infiltration over short distances and short time scales (Sawyer et. al., 2011; Stonedahl et al., 2013; Käser et al., 2013). Where the unconfined layer is small (e.g., in mountainous headwater streams with a rather small sediment layer overlying a hard-rock aquifer with relatively low hydraulic conductivity), the HZ is limited in its maximum extent, and travel times and distances are considerably shorter. However, in mountainous settings, slope angles are often much steeper due to erosion (here rivers incising into the bedrock) and further simulations are required to better understand the feedback between banks lope angle, hydraulic gradient and maximum extent of the unconfined layer allowing for reasonable river water infiltration. These simulations will also help us better understand the impact of bank slope on water supply and water quality to abstraction wells, e.g., used for the production of drinking water.

While the using the Boussinesq equation neglects the influence of the vadose zone, this approach as well as the assumption of vertically integrated distribution of hydraulic head have been widely used in the literature and proven adequate when simulating sinuosity-driven HEF patterns (Boano et al., 2006; 2010., Cardenas. 2008; 2009a, b; Gomez-Velez et al., 2012; 2017, Kruegler et al., 2020). While we found differences in HEF patterns when comparing simple models using the Boussinesq with those using Richard's equation (S4 in SI) these differences exist independent of using the DGM. However, we recommend in future studies to more systematically consider these two different approaches with respect to their advantages and limitations, e.g., in terms of

computability or efficiency in predicting HEF under various conditions. While in an ideal scenario a 3-D modeling approach includes vadose zone and riverbank slope angle (both variable in time and space), for the moment the implementation of such detailed models in practice suffers from limited computing capabilities.

5. Conclusions

The deformed geometry method was applied to characterize the expansion and contraction of hyporheic zones along sloping riverbanks, and to evaluate the impact of bank slope on hyporheic exchange flux, evolution of the HZ area and residence (travel) time distributions of the infiltrating water. To achieve this, several unconfined alluvial aquifers with varying slope angles and aquifer transmissivity values were simulated. Our results show that bank slope in a sinuosity-driven river was non-negligible when the aims of numerical/analytical models are the prediction of the evolution of the hyporheic zone during and after a flood event (transient flood forcing).

The overall findings of our work underline the need for including more realistic riverbank morphological conditions into simulations when studying lateral hyporheic exchange flow responses to dynamic forcings. Furthermore, our results show that more detailed information on bank slope (e.g., through more measurements) can lead to a better understanding of hyporheic flow patterns and potentially result in improved biochemical process understanding for real-world conditions for more complex morphological and depositional environments. Several conclusions can be drawn from our study:

1. Sloping riverbanks can considerably increase HEF during a flood event, especially when the river is connected to an alluvial aquifer with rather high hydraulic conductivity and small bank slope angles as water can more easily infiltrate the connected aquifer. Smaller bank slope angles can lead to an extended hyporheic zone with river water infiltrating deeper (penetration distance) into the aquifer.

However, bank slope has only a minor impact on the hyporheic outflow flux (water re-entering the stream).

2. During a flood event, the impact of bank slope on residence time distributions (RTD) is more pronounced for high transmissivity aquifers, due to the larger area and deeper penetration distance of the HZ for these conditions. On the contrary, the impact of bank slope on RTD for lower transmissivity aquifers is minor during the flood event, but bank slope can have a significant and long-lasting effect for post-flood conditions.
3. River sinuosity should be considered when assessing the impact of bank slope on RTD. Variable bank slope can lead to both longer and shorter residence times when compared to vertical riverbank conditions.
4. Bank slope has a greater impact on the residence time of hyporheic water in lower-transmissivity aquifers, thereby delaying the time of younger water discharge downstream of a meander bend, which also delays the outflow of older water upstream of that bend.

Code and data availability

Additional information regarding methodology and results is provided in the supporting information (SI).

Author contributions

YL: Conceptualization, Formal analysis, Methodology, Investigation, Writing

US: Conceptualization, Methodology, Writing

ZW: Funding acquisition, Software, Supervision

SK: Validation, Writing, Supervision

HL: Project administration, Supervision

Acknowledgements

This research was partially supported by the National Natural Science Foundation of China (Grant Numbers: 42272290, 41830862, and 42022018), and China Scholarship Council (CSC, 202106410042).

Competing interests

The authors declare that they have no conflict of interest.

References

Bear, J., and Cheng, A. H. D.: Modeling groundwater flow and contaminant transport, Vol. 23, pp. 83, Dordrecht: Springer, 2010.

Bertrand, G., Goldscheider, N., Gobat, J.-M., and Hunkeler, D.: Review: From multi-scale conceptualization to a classification system for inland groundwater-dependent ecosystems, Hydrogeology Journal, 20, 5-25, 2012.

Boano, F., Camporeale, C., Revelli, R., and Ridolfi, L.: Sinuosity-driven hyporheic exchange in meandering rivers, Geophysical Research Letters, 33, L18406, 2006.

Boano, F., Harvey, J. W., Marion, A., and Packman, A. I., Revelli, R., Ridolfi, L., and Wörman, A.: Hyporheic flow and transport processes: Mechanisms, models, and biogeochemical implications, Reviews of Geophysics, 52, 603-679, 2014.

Boano, F., Demaria, A., Revelli, R., and Ridolfi, L.: Biogeochemical zonation due to intrameander hyporheic flow, Water Resource. Research. 46, W02511, 2010.

Boano, F., Revelli, R., and Ridolfi, L.: Effect of streamflow stochasticity on bedform-driven hyporheic exchange. Advances in Water Resources, 33(11), 1367-1374. 2010.Boulton, A. J., Datry, T., Kasahara, T., Mutz, M., and Stanford, J. A.: Ecology and management of the hyporheic zone: Stream–groundwater interactions of running waters and their floodplains, Journal of the North American Benthological Society, 29 (1), 26-40, 2010.

Brunke, M., and Gonser, T.: The ecological significance of exchange processes between rivers and groundwater, Freshwater Biology, 37 (1), 1-33, 1997.

Cardenas, M. B.: The effect of river bend morphology on flow and timescales of surface water-groundwater exchange across pointbars, Journal of Hydrology, 362, 134-141, 2008.

Cardenas, M. B.: A model for lateral hyporheic flow based on valley slope and channel sinuosity, Water Resources Research, 45, W01501, 2009a.

Cardenas, M. B.: Stream-aquifer interactions and hyporheic exchange in gaining and

losing sinuous streams, Water Resources Research, 45, W06429, 2009b.

Cardenas, M. B.: Hyporheic zone hydrologic science: A historical account of its emergence and a prospectus, Water Resources Research, 51, 3601-3616, 2015.

Cooper, H. H., and Rorabaugh, M. I.: Ground-water movements and bank storage due to flood stages in surface streams, Report of Geological Survey Water-Supply, pp. 1536-J, US Government Printing Office, Washington, United States, 1963.

Derx, J., Farnleitner, A. H., Blöschl, G., Vierheilig, J., and Blaschke, A. P.: Effects of riverbank restoration on the removal of dissolved organic carbon by soil passage during floods–A scenario analysis, Journal of Hydrology, 512, 195-205, 2014.

Doble, R. C., Crosbie, R. S., Smerdon, B. D., Peeters, L., and Cook, F. J.: Groundwater recharge from overbank floods, Water Resources Research, 48 (9), W09522, 2012a.

Doble, R., Brunner, P., McCallum, J., and Cook, P. G.: An analysis of river bank slope and unsaturated flow effects on bank storage, Ground Water, 50 (1), 77-86, 2012b.

Donea, J., A. Huerta, J.-P. Ponthot, and A. Rodriguez-Ferran.: Arbitrary Lagrangian–Eulerian methods, In Encyclopedia of Computational Mechanics, ed. E. Stein, R. de Borst, and T. J. R. Hughes, 413-434. New York: John Wiley & Sons, 2004.

Duarte, F., Gormaz, R., and Natesan, S.: Arbitrary Lagrangian–Eulerian method for Navier–Stokes equations with moving boundaries, Computer Methods in Applied Mechanics and Engineering, 193 (45-47), 4819-4836, 2004.

Fox, G. A., and Wilson, G. V.: The role of subsurface flow in hillslope and stream bank erosion: a review, Soil Science Society of America Journal, 74 (3), 717-733, 2010.

Gao, Y., Zhu, B., Zhou, P., Tang, J. L., Wang, T., and Miao, C. Y.: Effects of vegetation cover on phosphorus loss from a hillslope cropland of purple soil under simulated rainfall: a case study in China, Nutrient Cycling in Agroecosystems, 85 (3), 263-273, 2009.

Gomez-Velez, J. D., and Harvey, J. W.: A hydrogeomorphic river network model predicts where and why hyporheic exchange is important in large basins,

773 Geophysical Research Letters, 41, 6403–6412, 2014.
774 Gomez-Velez, J. D., Wilson, J. L., and Cardenas, M. B.: Residence time distributions
775 in sinuosity-driven hyporheic zones and their biogeochemical effects, Water
776 Resources Research, 48 (9), 2012.
777 Gomez-Velez, J. D., Wilson, J. L., Cardenas, M. B., and Harvey, J. W.: Flow and
778 residence times of dynamic river bank storage and sinuosity-driven hyporheic
779 exchange, Water Resources Research, 53, 8572-8595, 2017.
780 Gomez-Velez, J. D., Harvey, J. W., Cardenas, M. B., and Kiel, B.: Denitrification in the
781 Mississippi River network controlled by flow through river bedforms, Nature
782 Geoscience, 8, 941-945, 2015.
783 Hagerty, D. J., Spoor, M. F., and Parola, A. C.: Near-bank impacts of river stage control,
784 Journal of Hydraulic Engineering, 121 (2), 196-207, 1995.
785 Hooke, J. M.: River meandering, In E. Wohl & J. Shroder (Eds.), Treatise on
786 geomorphology, Vol. 9, pp. 260-288, CA: Academic Press, San Diego, 2013.
787 Hester, E. T., and Gooseff, M. N.: Moving beyond the banks: Hyporheic restoration is
788 fundamental to restoring ecological services and functions of streams,
789 Environmental Science and Technology, 44 (5), 1521-1525, 2010.
790 Hunt, B.: An approximation for the bank storage effect, Water Resources Research, 26
791 (11), 2769–2775, 1990.
792 Hunter, K, S., Wang, Y., Van, C, P.: Kinetic modeling of microbially-driven redox
793 chemistry of subsurface environments: coupling transport, microbial metabolism
794 and geochemistry. Journal of hydrology, 209 (1-4), 53-80, 1998.
795 Käser, D. H., Binley, A., and Heathwaite, A. L.: On the importance of considering
796 channel microforms in groundwater models of hyporheic exchange. River
797 Research and Applications, 29(4), 528-535, 2013.
798 Kiel, B. A., Cardenas, M. B.: Lateral hyporheic exchange throughout the Mississippi
799 River network, Nature Geoscience, 7 (6), 413-417, 2014.
800 Krause, S., Abbott, B. W., Baranov, V., Bernal, S., Blaen, P., Datry, T., Drummond, J.,

Fleckenstein, J. H., Gomez-Velez, J., Hannah, D. M., Knapp, J. L. A., Kurz, M., Lewandowski, J., Marti, E., Mendoza-Lera C., Milner, A., Packman, A., Pinay, G., Ward, A. S., Zarnetzke, J. P.: Organizational principles of hyporheic exchange flow and biogeochemical cycling in river networks across scales, Water Resources Research. 58, e2021WR029771, 2022.

Krause, S., Hannah, D. M., Fleckenstein, J. H., Heppell, C. M., Pickup, R., Pinay, G., Robertson, A. L., and Wood, P. J.: Inter-disciplinary perspectives on processes in the hyporheic zone, Ecohydrology Journal. 4 (4), 481-499, 2011.

Krause, S., Lewandowski, J., Grimm, N., Hannah, D. M., Pinay, G., Turk, V., Argerich, A., Sabater, F., Fleckenstein, J., Schmidt, C., Battin, T., Pfister, L., Martí, E., Sorolla, A., Larned, S., and Turk, V.: Ecohydrological interfaces as critical hotspots for eocsystem functioning, Water Resources Research. 53, 6359-6376, 2017.

Krause, S., Tecklenburg, C., Munz, M., and Naden, E.: Streambed nitrogen cycling beyond the hyporheic zone: Flow controls on horizontal patterns and depth distribution of nitrate and dissolved oxygen in the upwelling groundwater of a lowland river, Journal of Geophysical Research: Biogeosciences, 118 (1), 54-67, 2013.

Kruegler, J., Gomez-Velez, J. D., Lautz, L. K., and Endreny, T. A.: Dynamic evapotranspiration alters hyporheic flow and residence times in the intrameander zone, Water, 12 (2), 424, 2020.

Larkin, R. G., and Sharp, J. M.: On the relationship between river-basin geomorphology, aquifer hydraulics, and groundwater flow direction in alluvial aquifers, Geological Society of America Bulletin, 104, 1608-1620, 1992.

Laubel, A., Kronvang, B., Hald, A. B., and Jensen, C.: Hydromorphological and biological factors influencing sediment and phosphorus loss via bank erosion in small lowland rural streams in Denmark. Hydrological processes, 17(17), 3443-3463, 2003.

Li, H., Boufadel, M. C., and Weaver, J. W.: Quantifying bank storage of variably saturated aquifers, Ground Water, 46 (6), 841-850, 2008.

Liang, X. Y., Zhan, H. B., and Schilling, K.: Spatiotemporal responses of groundwater flow and aquifer-river exchanges to flood events, Water Resources Research, 54 (3), 1513-1532, 2018.

Lindow, N., Fox, G. A., and Evans, R. O.: Seepage erosion in layered stream bank material, Earth Surface Processes and Landforms, 34 (12), 1693-1701, 2009.

Mayor, Á. G., Bautista, S., Small, E. E., Dixon, M., and Bellot, J.: Measurement of the connectivity of runoff source areas as determined by vegetation pattern and topography: A tool for assessing potential water and soil losses in drylands, Water Resources Research, 44 (10), 2008.

Maury, B.: Characteristics ALE method for the unsteady 3D Navier-Stokes equations with a free surface, International Journal of Computational Fluid Dynamics, 6 (3), 175-188, 1996.

McCallum, J.L., P.G. Cook, P. Brunner, and D, Berhane.: Solute dynamics during bank storage flows and implications for chemical baseflow separation, Water Resources Research, 46: W07541, 2010.

McClain, M. E., Boyer, E. W., Dent, C. L., Gergel, S. E., Grimm, N. B., Groffman, P. M., Hart, S. C., Harvey, J. W., Johnston, C. A., Mayorga, E., Mcdowell, W and Pinay, G.: Biogeochemical hot spots and hot moments at the interface of terrestrial and aquatic ecosystems, Ecosystems, 6 (4), 301-312, 2003.

Millar, R. G., and Quick, M. C.: Effect of bank stability on geometry of gravel rivers, Journal of Hydraulic Engineering, 119 (12), 1343-1363, 1993.

Millington, R. J., and Quirk, J. P.: Permeability of porous solids, Transactions of the Faraday Society, 57, 1200-1207, 1961.

Osman, A. M., and Thorne, C. R.: Riverbank stability analysis. I: Theory, Journal of Hydraulic Engineering, 114 (2), 134-150, 1988.

Pinay, G., Peiffer, S., De Dreuzy, J. R., Krause, S., Hannah, D. M., Fleckenstein, J. H.,

857 Sebilo, M., Bishop, K., and Hubert-M, L.: Upscaling nitrogen removal capacity
858 from local hotspots to low stream orders' drainage basins, Ecosystems, 18 (6),
859 1101-1120, 2015.
860 Pohjoranta, A., and Tenno, R.: Implementing surfactant mass balance in 2D FEM–ALE
861 models, Engineering with Computers, 27 (2), 165-175, 2011.
862 Puttock, A., Macleod, C. J., Bol, R., Sessford, P., Dungait, J., and Brazier, R. E.:
863 Changes in ecosystem structure, function and hydrological connectivity control
864 water, soil and carbon losses in semi-arid grass to woody vegetation transitions,
865 Earth Surface Processes and Landforms, 38 (13), 1602-1611, 2013.
866 Seminara, G.: Meanders, Journal of Fluid Mechanics, 554, 271-297, 2006.
867 Schmadel, N. M., A. S. Ward, C. S. Lowry, and J, M. Malzone.: Hyporheic exchange
868 controlled by dynamic hydrologic boundary conditions, Geophysical Research
869 Letters, 43, 4408-4417, 2016.
870 Sawyer, A. H., Bayani Cardenas, M., and Buttles, J.: Hyporheic exchange due to
871 channel-spanning logs. Water Resources Research, 47(8), 2011.
872 Sharp, J. M.: Limitations of bank-stopage model assumptions, Journal of Hydrology,
873 35 (1-2), 31-47, 1977.
874 Siergieiev, D., Ehlert, L., Reimann, T., Lundberg, A., and Liedl, R.: Modelling
875 hyporheic processes for regulated rivers under transient hydrological and
876 hydrogeological conditions, Hydrology and Earth System Sciences, 19 (1), 329-
877 340, 2015.
878 Singh, T., Gomez‐Velez, J. D., Wu, L., Wörman, A., Hannah, D. M., and Krause, S.:
879 Effects of successive peak flow events on hyporheic exchange and residence times,
880 Water Resources Research, 56 (8), e2020WR027113, 2020.
881 Singh, T., Wu, L., Gomez-Velez, J. D., Lewandowski, J., Hannah, D. M., Krause, S.:
882 Dynamic hyporheic zones: Exploring the role of peak flow events on bedform-
883 induced hyporheic exchange, Water Resources Research, 55, 218-235, 2019.
884 Stonedahl, S. H., Harvey, J. W., and Packman, A. I.: Interactions between hyporheic

885 flow produced by stream meanders, bars, and dunes, Water Resources Research,
886 49, 5450-5461, 2013.
887 Trimble, S. W.: Erosional effects of cattle on streambanks in Tennessee, USA. Earth
888 surface processes and landforms, 19(5), 451-464, 1994.
889 Triska, F. J., Kennedy, V. C., Avanzino, R. J., Zellweger, G. W., and Bencala, K. E.:
890 Retention and transport of nutrients in a third - order stream in northwestern
891 California: Hyporheic processes, Ecology, 70 (6), 1893-1905, 1989.
892 Van Genuchten, M. T.: A closed - form equation for predicting the hydraulic
893 conductivity of unsaturated soils. Soil science society of America journal, 44(5),
894 892-898, 1980.
895 Weatherill, J. J., Atashgahi, S., Schneidewind, U., Krause, S., Ullah, S., Cassidy, N.,
896 and Rivett, M. O.: Natural attenuation of chlorinated ethenes in hyporheic zones:
897 A review of key biogeochemical processes and in-situ transformation potential,
898 Water research, 128, 362-382, 2018.
899 Wondzell, S. M., and Swanson, F. J.: Floods, channel change, and the hyporheic zone,
900 Water Resources Research, 35 (2), 555-567, 1999.
901 Wu, L., Gomez - Velez, J. D., Krause, S., Singh, T., Wörman, A., and Lewandowski, J.:
902 Impact of flow alteration and temperature variability on hyporheic exchange,
903 Water Resources Research, 56 (3), e2019WR026225, 2020.
904 Wu, L., Gomez-Velez, J. D., Krause, S., Wörman, A., Singh, T., Nützmann, G., and
905 Lewandowski, J.: How daily groundwater table drawdown affects the diel rhythm
906 of hyporheic exchange, Hydrology and Earth System Sciences, 25 (4), 1905-1921,
907 2021.
908 Wu, L., Singh, T., Gomez - Velez, J. D., Nützmann, G., Wörman, A., Krause, S., and
909 Lewandowski, J.: Impact of dynamically changing discharge on hyporheic
910 exchange processes under gaining and losing groundwater conditions, Water
911 Resources Research, 54 (12), 10-076, 2018.
912 Zarnetske, J. P., Haggerty, R., Wondzell, S. M., and Baker, M. A.: Dynamics of nitrate

913 production and removal as a function of residence time in the hyporheic zone,
914 Journal of Geophysical Research, 116, G01025, 2021.
915 Zarnetske, J. P., Haggerty, R., Wondzell, S. M., Bokil, V. A., and González-Pinzón, R.:
916 Coupled transport and reaction kinetics control the nitrate source-sink function of
917 hyporheic zones, Water Resources Research, 48, W11508, 2012.
918 Zingg, A. W.: Degree and length of land slope as it affects soil loss in run-off,
919 Agricultural Engineering, 21, 59-64, 1940.
920